AIAA AVIATION Forum
June 25-29, 2018, Atlanta, Georgia
2018 Joint Thermophysics and Heat Transfer Conference

10.2514/6.2018-4178

Methodology for Optimal Design of a Conformal Ablative Heatshield

Adam T. Sidor*
Georgia Institute of Technology, Atlanta, GA, 30332

Robert D. Braun†
University of Colorado, Boulder, CO, 80309

Graeme J. Kennedy‡
Georgia Institute of Technology, Atlanta, GA, 30332

Conformal ablators are low density composite materials comprised of a flexible fibrous substrate and polymer matrix. Recent advancements have improved the efficiency of conformal ablator fabrication through vacuum infusion processing where resin is directly injected into a fiber substrate enclosed in a matched mold. This mold filling process can be numerically simulated to inform mold and process design. An automated methodology pairing a mold filling simulation with an approach for tiling a heatshield geometry leads to designs optimized for manufacturing. Material property estimation generalizes the approach to a range of constituent materials, enabling rapid conceptual evaluation of a conformal ablative heatshield. This work improves on the state of the art which relies on heuristic methods tailored to a particular material and aeroshell geometry. Results for a 4.5 meter, 70 degree sphere-cone aeroshell demonstrate the power of an integrated approach.

Nomenclature

K	Permeability
L_{sub}	Raw substrate length
M	Number of OML segments
N	Number of tiles
N_{lb}	Lower bound on N
N_{ub}	Upper bound on N
P	Pressure
P_{atm}	Atmospheric pressure
P_{vap}	Vapor pressure
P_{vent}	Vent pressure
Q	Number of rings in OML segment
R	Radius of Curvature
R_{gate}	Gate radius
T_f	Time to fill
W_{sub}	Raw substrate width
Y	Char yield
d	Diameter
f	Fill factor
$f_{\text{obj},1}$	Tile layout objective function
$f_{\text{obj},2}$	Mold design objective function
l	Side length of tile or substrate

*Graduate Research Assistant, Guggenheim School of Aerospace Engineering, AIAA Student Member.
†Dean, College of Engineering and Applied Science, AIAA Fellow.
‡Assistant Professor, Guggenheim School of Aerospace Engineering, AIAA Senior Member.

p	Perimeter distance
p'	Blocked perimeter length
p_{total}	Total perimeter length
q	Volumetric flux
r	Radial coordinate
t	Thickness
t_{TPS}	TPS thickness
v	Macroscopic flow velocity
w	Weight fraction
x	Mole fraction
z	Height coordinate
$\left(\frac{\Delta l}{l}\right)_{\text{IP}}$	Length change (in plane)
$\left(\frac{\Delta l}{l}\right)_{\text{TT}}$	Length change (through thickness)
$\Delta\rho$	Density variation
Δt	Thickness variation
Γ_{gate}	Angular gate location (non-dimensional)
α	Geometry-dependent parameter (permeability)
β	Seam angle
γ	Angular span of tile or substrate
λ_{gate}	Radial gate location (non-dimensional)
μ	Dynamic viscosity
ν	Kinematic viscosity
ϕ	Porosity
ϕ_p	Percolation threshold
ρ	Density
LCM	Liquid Composite Molding
OML	Outer Mold Line
PICA	Phenolic Impregnated Carbon Ablator
SIRCA	Silicone Impregnated Reusable Ceramic Ablator
TPS	Thermal Protection System
VBI	Viscosity Blending Index
VIP	Vacuum Infusion Process (or Processing)

Subscripts

c	Component of resin solution
i	OML segment index
j	Ring index
comp	Property of the composite TPS material
fiber	Property of a fiber comprising the substrate
resin	Property of the cured resin
sol	Property of the resin solution
sub	Property of the substrate

Superscripts

f	Substrate dimension when flattened (for tile layout)
max	Maximum value
min	Minimum value
post	Post-process property
pre	Pre-process property
sub	Substrate dimension (for tile layout)

I. Introduction

Conformal ablators are a recent advancement on rigid ablative thermal protection system (TPS) materials that utilize a flexible fibrous substrate, rather than the rigid substrates of Phenolic Impregnated Carbon Ablator (PICA) and related materials. Substrates, such as felts or battings, are impregnated with

polymer resin in a mold to yield a rigid near net shape part. The lack of fiber connectivity through the thickness enables the TPS to tolerate larger strains than comparable rigid substrate ablators facilitating larger tiles and installation on most aeroshells without strain isolation. The development of these materials is documented in several references.[1–10] Resins are substantially diluted to control resin loading and allow infusion at lower pressures. The resulting material is lightweight and porous. Several conformal TPS variants have been developed including conformal analogs of PICA and SIRCA (Silicone Impregnated Reusable Ceramic Ablator).[3,10] Recent work has focused on identifying thicker and higher density carbon felt substrates.[7]

Conformal ablative materials are fabricated using an open liquid impregnation process adapted from PICA processing.[5,7] No computational tool exists to assist process and mold design. Mold design is based on experience and trial and error. These designs are evaluated through experimentation, which can be costly if the mold needs to be modified or redesigned. In addition, the current process wastes a significant portion of resin (potentially up to half). Some resin necessarily remains outside the substrate, getting cured along with the part only to be removed and discarded post–process adding to labor and cost. Vacuum infusion processing (VIP) – a type of liquid composite molding (LCM) – improves processing efficiency and enables numerical process design.[11] VIP draws resin into a fibrous substrate enclosed within an evacuated mold. Mold filling can be simulated using Darcy's law – an approach that has been rigorously developed for LCM processes.[12] Such a capability allows evaluation of mold and process design in advance leading to improved material quality and reduced experimental burden. Dry spot formation, and subsequent voids, can be identified and avoided prior to tool fabrication.

This work outlines a methodology for the design of a conformal ablative heatshield, pairing a Darcy's law simulation of mold filling with a tiling procedure to divide the geometry into manufacturable segments. The methodology proceeds in three sequential steps: (1) tiling the heatshield, (2) designing a mold to fabricate each tile, and (3) estimating relevant properties of the fabricated TPS material. Optimization tailors the tile layout to VIP processing, minimizing the total number of tiles while meeting manufacturing constraints (e.g., substrate size). In the mold design step, gate and vent locations are located to avoid dry spot formation. Lastly, selected properties of the fabricated TPS are estimated allowing evaluation of process and/or material changes. To generalize the methodology to other material formulations, certain required inputs (resin, substrate, and composite properties) are approximated using simplified material models. Estimating these properties, for which experimental data may not exist, reduces reliance on experimental results and speeds conceptual design. For example, the effect of a change in substrate can be evaluated without repeated processing, sampling, and testing of the new material.

A rigorous design methodology that integrates material selection, tile layout and processing over segregated, ad hoc approaches improves on the state of the art, which relies on a largely manual approach tailored to a specific material and aeroshell geometry. Instead, heatshields can be automatically generated for a range of materials and geometries reducing design time. Optimal mold designs can ensure consistent, high quality parts. The designer is freed to evaluate other aspects of heatshield design such as TPS material composition and its impact on processing and properties. Results for a 4.5 meter, 70 degree sphere-cone, conformal PICA heatshield demonstrate the flexibility and capability of the integrated methodology.

II. Gap Analysis and Solution

A. Gap Analysis: Conventional Manufacturing and Design

Conformal ablators are manufactured using a liquid impregnation technique based on PICA processing.[5,7,13] In these processes, the fiber substrate is constrained in a matched mold and infiltrated by liquid resin in an open container while under vacuum. The process is carried out slowly (up to several hours for large parts) to ensure complete infiltration. The immersed part is cured at high temperature, removed from the container, and extracted from the now rigid resin. Removing excess resin requires careful cleaning and proper disposal – a time– and labor–intensive process. Once extracted, the bare part is heated a second time to remove residual solvent. This work addresses two shortcomings with the state-of-the-art process: (1) the large amount of excess, wasted resin inherent with open processing, and (2) the lack of a computational tool to support manufacturing.

Figure 1. Open mold used in state-of-the-art processing of conformal ablators (Credit: Ref. 5).

1. Manufacturing Inefficiency

Open processing is inherently inefficient. Openings in and around the mold are required to ensure adequate resin infiltration. An example is depicted in Figure 1. Note small and large openings in the top and around the perimeter of the mold that allow resin to enter the part from the surrounding container. Excess resin necessarily remains outside the substrate only to be discarded after curing. Up to roughly half of the resin may be wasted. This excess not only adds to direct material costs but impacts other aspects of processing as well. Resin removal is a messy and laborious process. Resins are often hazardous requiring careful cleaning and appropriate handling and disposal. The large amount of hazardous waste generated by the current process significantly burdens both the processing technician and waste disposal facilities. Thus, inefficiency cumulatively affects manufacturing leading to added labor, time, and cost.

2. Lack of a Design Tool

Mold design is a trial and error process informed by operator experience. No computational tool exists to support design and, thus, each new TPS geometry requires substantial design effort. Without a numerical tool, sizing and locating mold openings relies on best practices and engineering intuition but is not simulated prior to fabrication. Thus, non-optimal mold designs can only be identified after fabrication and subsequent material characterization. Mold fabrication requires substantial upfront investment, and modifications to a tool may be costly or even impossible. Additionally, because a single processing run takes several days from start to finish, iterations incur a steep penalty on manufacturing time and cost.

Tile layout, which is coupled to manufacturing, also impacts processing. Tiles must be manufacturable while meeting design and process restrictions. Again, without a computational tool, these criteria are manually incorporated into heatshield design and then translated to tooling and processing. A change in material composition (e.g., alternate substrate dimensions) will necessitate a change to tile geometry and subsequent mold design.

Finally, no framework exists for evaluating final TPS material properties and their uncertainties, which are important for sizing a TPS, relative to its constituents. Substrates in conformal ablators are inherently variable (in thickness and density) and produce subsequent variability in the final TPS. The current approach relies on experimentally accumulating properties across many TPS samples and quantifying uncertainty through statistical analysis. This method is time intensive and cannot easily account for changes in constituent materials.

B. Solution: Vacuum Infusion Processing and Simulation

Vacuum infusion processing improves on the state of the art by injecting resin directly into a fiber substrate within a mold.[11] Like the state-of-the-art process, VIP proceeds in three steps: resin infusion (also called mold filling), curing, and drying (Figure 2). However, VIP is carried out within a closed, rather than open, mold. The substrate is first draped and enclosed within the rigid mold. Vacuum pulled on the mold cavity at the vent draws resin into the substrate at an inlet, or gate, filling the part (Step 1). Full saturation is critical. If gas becomes entrapped within the part during mold filling, infusion will be incomplete and voids

may occur in the TPS material. Once the substrate is saturated, plugs sealing the mold top are removed and a secondary lid installed to enclose the cavity above the part (Step 2). This assembly is then heated to cure the resin. As the material heats up, excess resin expands into the upper cavity and cures there. After curing, the excess is removed and discarded, the secondary lid is re-installed, and the mold is subjected to a second heating cycle to remove residual solvent and dry the part (Step 3). Inert gas flows through the mold during both curing and drying, preventing resin oxidation and carrying away volatile compounds generated during processing.

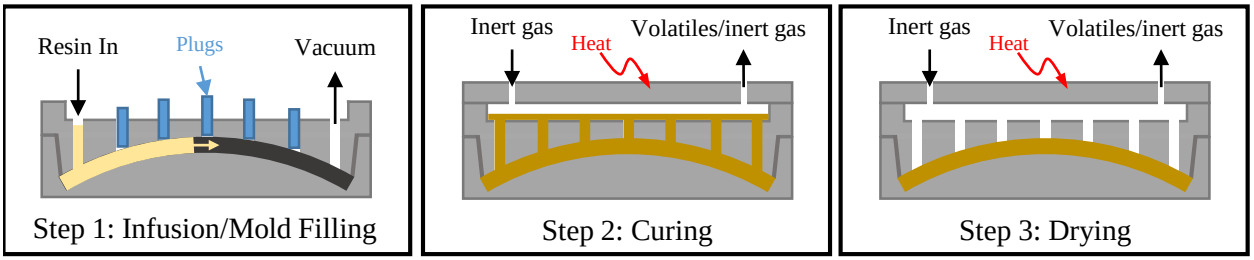

Figure 2. Vacuum infusion processing of conformal ablators.

Vacuum infusion processing addresses the shortcomings of the state-of-the-art process. First, it improves manufacturing efficiency through the use of a closed, rather than open, process. Not only does this approach eliminate almost all resin waste, a direct cost reduction over the current process, it significantly simplifies part clean up. While VIP does not eliminate all waste, it is substantially reduced. With a well-designed mold, clean up is on the order of a few minutes, rather than an hour or more, and waste is only a few percent of the total.

Second, mold filling can be numerically simulated using Darcy's Law, an empirical law describing flow through porous media. Numerical implementations of Darcy's Law have enabled mold and process design in a variety of LCM processes: RTM,[14] VaRTM,[15] vacuum infusion,[16] and SCRIMP[17] among many others. In the literature, numerical simulation is frequently employed to optimize gate and vent locations.[18–20] Elsewhere, a numerical approach optimized injection flow rate to minimize microscopic and macroscopic voids.[21] In addition to design, modeling has enabled real time process monitoring and control.[22] Application of Darcy's law to LCM is itself an extension of established work in soil mechanics and groundwater flows[23] originating with Darcy himself.

The law, an empirical relation describing flow through a porous medium, relates macroscopic fluid flow velocity to pressure gradient. The porous material is represented as a continuum with: porosity, ϕ, and permeability, K. In one dimension, Darcy's law is written

$$q = -\frac{K}{\mu}\frac{\mathrm{d}P}{\mathrm{d}x} \tag{1}$$

where μ is the dynamic viscosity of the infiltrating fluid, q is an average volumetric flux[a] and $\frac{\mathrm{d}P}{\mathrm{d}x}$ is a pressure gradient. Dividing Eq. 1 by porosity yields an expression for the average flow velocity through the medium,

$$v = -\frac{K}{\phi\mu}\frac{\mathrm{d}P}{\mathrm{d}x} \tag{2}$$

Thus, modeling mold filling via Darcy's law requires knowledge of three material quantities: ϕ and K of the porous medium and μ of the liquid infiltrant as well as the pressure field within the saturated medium. The latter is obtained by combining Darcy's Law with conservation of mass to yield an elliptic partial differential equation governing the saturated region.

A Darcy's law simulation can identify potential mold dry spots, ensuring well-infused TPS with no voids. However, a conformal heatshield consists of multiple tiles each requiring a potentially unique mold design. Therefore, connecting the mold filling simulation with a tile layout tailored to VIP yields a design optimized for manufacturing. The result is a tiled heatshield and the mold designs required to fabricate it. By also estimating material properties, the resulting TPS material can be assessed, enabling complete, automated

[a]With units of volume per time per area, or simply length per time

design from geometry to manufacturing to properties. Such a methodology – the coupling of tile layout, process design, and material property estimation – is the subject of this work, forming the backbone of a conceptual framework for making and evaluating conformal ablative TPS materials.

In short, the VIP approach simultaneously improves both manufacturing and design capabilities for conformal TPS materials. The process is efficient (generating significantly less waste than the current process and requiring less hands on labor) and numerical simulation enables optimal mold design (ensuring high quality, well-infused TPS) and forms the basis for a powerful conceptual design tool for engineers. This tool allows rapid evaluation of changes to constituent materials, process parameters, and TPS geometry and their impact on manufacturing and TPS properties. An overview of the methodology is presented next.

III. Design Methodology

The design methodology combines a Darcy's law simulation of the mold filling process with tile layout and material property estimation to produce an optimal manufacturing design. It encompasses three sequential tasks: (1) generating a tile layout for the specified heatshield geometry, (2) producing a VIP mold design for each tile geometry, and (3) estimating relevant properties of the fabricated TPS material. These design tasks form the core of the methodology (Figure 3). Iteration occurs within the tiling and mold design tasks converging on an optimal solution before proceeding to the next step. Required inputs to the methodology precede the design tasks. These are differentiated into primary and secondary inputs. The former are quantities or aspects of the design that must be known a priori (though approaches for obtaining these quantities are suggested below) while the latter can be estimated to simplify early conceptual design where experimental data may be scarce. In the figure, outcomes of each step are listed below each heading and are discussed in corresponding sections below. Before proceeding to a detailed description of the methodology, a few notes will be made on the limitations of what is presented here.

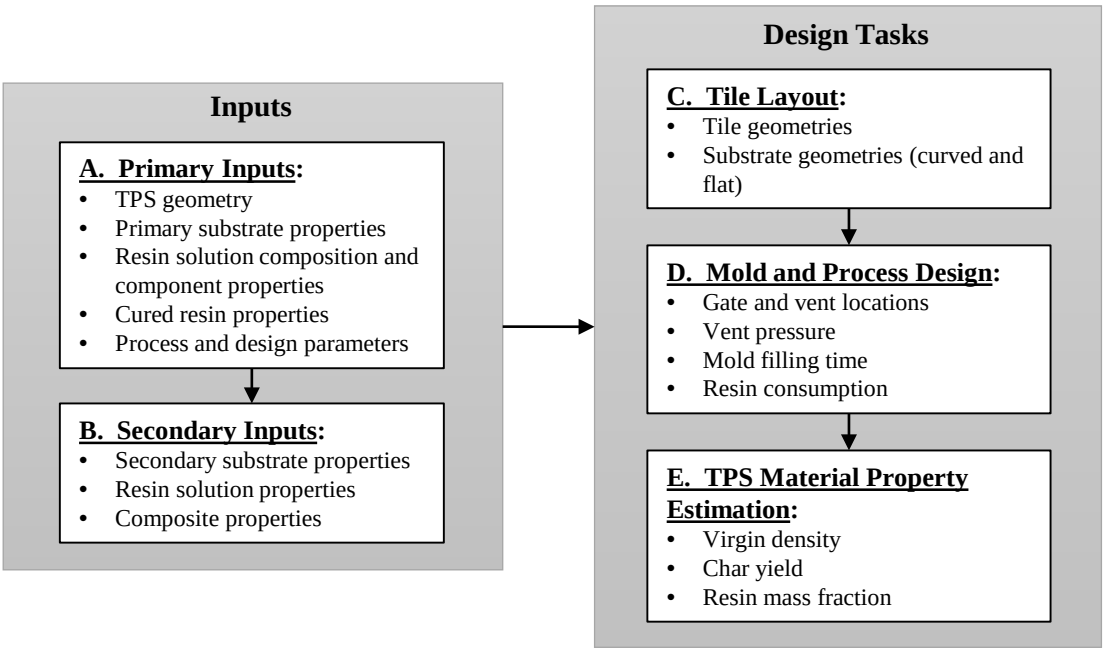

Figure 3. Design methodology for tiling and fabricating a conformal heat shield.

First, the tiling procedure described considers symmetric designs only, which is appropriate for zero angle of attack trajectories with the stagnation point on the nose of the vehicle. An offset stagnation point, and correspondingly asymmetric tile layout, is not considered. TPS geometry is limited to conical aeroshells with a blunted, spherical nose, and uniform TPS thickness is assumed. While this limits the scope of the current work, the methodology itself can be expanded to different geometries and asymmetric layouts. Similar design rules could be implemented to address these cases. Alternatively, the tile layout could be generated using

an external process and used as an input to the methodology. In that case, care must be taken that the tile layout is suited to the VIP process. For reasons that will become clear below, the number of unique tile geometries should be minimized to limit the number of molds that must be fabricated. In either case, tiling is decoupled from VIP simulation allowing tile layout rules to be modified without change to the rest of the methodology.

Second, the mold filling simulation considers single gate, single vent mold designs. Injection occurs at a point (though the gate is modeled as a two-dimensional circular source). More complicated gate designs are possible (e.g., a line source) but are not considered here, nor are multiple gate solutions. While these designs may improve processing for more complex composite parts, they complicate the flow simulation and are likely not necessary for the relatively simple geometries typical of TPS tiles. Experimental work has demonstrated single gate designs to be sufficient for the TPS materials and geometries under consideration here. Other minor limitations of the methodology are discussed within the relevant sections.

A. Primary Inputs / Known Quantities

Primary inputs to the methodology are outlined below. These inputs include both design inputs (TPS geometry), material inputs (properties of the constituent materials), and process and design parameters. These inputs must be known or determined a priori from external sources or analyses. Certain quantities, such as the viscosities and vapor pressures of the resin components, can be obtained from reference materials. Other quantities, such as substrate density and dimensions, are generally available from the manufacturer. The fiber density and fiber diameter for a specific substrate material is not generally available but can be approximated based on fiber type. Still other properties, namely the cured resin density, pose more of a challenge. Resin density varies with initial resin composition and process conditions, and it is also coupled to the shrinkage of the material during processing.

1. TPS Geometry

TPS geometry is specified as a two-dimensional outer mold line (OML) geometry and a TPS thickness. Ideally, a given geometry should be feasible for manufacturing. For example, the desired TPS thickness must not exceed that which is achievable with the specified substrate and any curvature should not be less than a minimum radius of curvature to ensure uniform draping of the substrate without wrinkling (drapeability, considered below). The methodology identifies such infeasibilities but requires the designer to supply an alternate material or a different manufacturing technique to rectify them.

2. Substrate Properties

Bulk Properties Required substrate properties include those of the bulk material – density, ρ_{sub}, and dimensions (width, W_{sub}, length, L_{sub}, and thickness, t_{sub}). Fiber substrates are only available, or manufacturable, in certain sizes. For example, the carbon felt used in C-PICA is available up to a thickness of about 1 inch and a width of 41–47 inches. Additionally, there is inherent variability in substrate properties. Of interest here are variation in the density, $\Delta\rho_{\text{sub}}$, and thickness, Δt_{sub}, which drive variation in the final TPS material. For off-the-shelf materials, this data is generally well known and published in material datasheets.

Fiber Properties Properties of the the individual fibers composing the substrate – fiber density, ρ_{fiber} and diameter, d_{fiber} – are less available but can be approximated for carbon fiber materials given a known precursor. Rayon-based carbon fibers, typical in ablative TPS due to low thermal conductivity, historically range in density from 1.40 g/cc to 1.80 g/cc though the upper end encompasses high modulus fibers that are no longer manufactured.[24] Current commercially available fibers fall in a narrower range (1.35 g/cc to 1.44 g/cc),[25] and fiber diameters are around 10 μm.[26]

Drapeability Drapeability is the ability of a fabric to conform to a desired shape. High curvature can lead to wrinkling and unpredictable, and undesirable, mold flow behavior called racetracking. In addition, wrinkles reduce usable thickness. Draping, and wrinkling, of fabric materials are complex phenomena influenced by both microscopic and macroscopic properties. Modeling draping in LCM is an area of considerable research in itself. A pin-joint model, which assumes fibers are pinned together at intersections, is frequently used to predict deformation and wrinkling of woven materials.[27] Other work has addressed how draping changes substrate permeability.[28]

This work ensures uniform draping, i.e., no substrate wrinkling, by enforcing a minimum radius of curvature constraint, $R^{\min}$. If the curvature of a tile violates this constraint, then it cannot be fabricated using the current process, and an alternate process or material must be selected. Here, $R^{\min}$ must be measured or computed a priori. Future work will seek to estimate this quantity rather than requiring it as an input.

3. Resin Solution Composition and Component Properties

Resin solutions are a mixture of components including resin, solvent, and potentially other fillers. The methodology requires two properties of the resin solution, dynamic viscosity and vapor pressure, both important parameters for mold filling. Mixture quantities can be estimated using weighted averaging of its components. Thus, in addition to resin composition itself (e.g., relative component amounts by weight and by mole), individual component properties must be known: viscosity (either the kinematic viscosity, ν, or dynamic viscosity, μ), vapor pressure, P_{vap}, and density of each component must be supplied.

4. Cured Resin Properties

Density and Dimensional Changes The resin undergoes both mass and volume change during processing. Mass loss occurs due to evaporation of solvent and/or reaction products. Volume change occurs as the solution expands due to heating and contracts due to crosslinking. Contraction of the resin system is coupled to the substrate present (which may resist shrinkage and prevent some or all contraction) and mold boundary conditions (bonding to the mold walls also prevents contraction). All of these factors must be considered in the analysis of post-process resin properties. The methodology requires cured resin density and its volumetric shrinkage during processing. Note that these are properties of the pure resin where there is no resistance to volume change. This restriction will not hold in practice. However, these quantities can bound real-world results. An experimental approximation can be made by curing a given resin within a container possessing non-bonding walls. For example, PTFE coating, with its chemical resistance and non-stick properties, can achieve the desired boundary conditions. The necessary quantities are then obtained from measurement of pre- and post-cured mass and dimensions.

Char Yield Resin char yield, Y_{resin}, is highly dependent on composition and processing. This quantity may be measured experimentally. However, in the absence of experimental results, historical data may be useful (e.g., as compiled by Williams and Curry[29] and Parker and Winkler[30]). The latter reference contains char data for phenolic resins. It may also be estimated using computational techniques. For example, Parker and Winkler present a method for predicting phenolic char yield as a function of resin composition and degree of crosslinking. A similar approach is presented by Wang, et al.[31] Still other work uses a kinetics model of phenolic pyrolysis to predict char formation.[32]

5. Process and Design Parameters

Gate Design Gate design includes geometry and an appropriate boundary condition to reflect the process setup, typically either a constant pressure or constant flow rate condition.[33] This work uses a constant pressure boundary condition with gate pressure set to the ambient atmospheric pressure, P_{atm}, to reflect the process set up.

Minimum Seam Angle A minimum seam angle, $\beta^{\min}$, prevents seam alignment between adjacent tiles, a requirement typical of tiled heatshields (e.g., see the Mars Science Laboratory heatshield[34]). $\beta^{\min}$ is enforced during tile layout.

B. Secondary Inputs / Computed Quantities

The second set of properties are intermediate material properties – properties that are functionally dependent on those above and are required for subsequent mold filling analysis and TPS property estimation. They are divided into properties of the substrate, properties of the resin solution, and properties of the combined substrate and resin after processing (i.e., the composite). Any of these properties may be experimentally measured and treated as additional inputs to the methodology (which is done in a few cases here pending

future work). As a result, some inputs identified above may no longer be required. Alternatively, these properties can be numerically estimated using simplified material models to speed design evaluation.

1. *Substrate Properties*

Substrate properties are estimated assuming an idealized model, the filamentary analog method, which treats the material as a three-dimensional network of smooth, nonporous, randomly oriented fibers with constant radius, d_{fiber}, and density, ρ_{fiber}.[11]

DENSITY Note that multiple substrate densities appear in this methodology: the nominal, uncompressed density specified above, ρ_{sub}; the compressed density in the mold prior to processing, $\rho_{\text{sub}}^{\text{pre}}$; and the density after processing, $\rho_{\text{sub}}^{\text{post}}$. Practically, molds must be designed to the minimum substrate thickness to ensure there are no gaps between the fiber material and the tooling, which can lead to racetracking. Therefore, the uncompressed substrate, with thickness variance Δt_{sub}, is compressed to a uniform thickness of $t_{\text{sub}} - \Delta t_{\text{sub}}$. Assuming a constant areal density, then, the compressed, pre-process density is

$$\rho_{\text{sub}}^{\text{pre}} = \frac{\rho_{\text{sub}} t_{\text{sub}}}{t_{\text{sub}} - \Delta t_{\text{sub}}} \tag{3}$$

The substrate contracts during processing leading to a further increase in the density:

$$\rho_{\text{sub}}^{\text{post}} = \frac{\rho_{\text{sub}}^{\text{pre}}}{\left[1 - \left(\frac{\Delta l}{l}\right)_{\text{IP}}\right]^2 \left[1 - \left(\frac{\Delta l}{l}\right)_{\text{TT}}\right]} \tag{4}$$

where $\left(\frac{\Delta l}{l}\right)_{\text{TT}}$ and $\left(\frac{\Delta l}{l}\right)_{\text{IP}}$ denote through thickness and in plane shrinkage during processing – quantities described below.

POROSITY Porosity is estimated by a ratio of bulk substrate density, ρ_{sub}, to the density of an individual fiber, ρ_{fiber},

$$\phi = 1 - \frac{\rho_{\text{sub}}}{\rho_{\text{fiber}}} \tag{5}$$

Substrate porosity changes during processing due to material shrinkage (porosity decreases as the material shrinks). Pre- and post-process porosity is denoted by appropriate superscripts. Note also that the post-process porosity does not refer to the porosity of the composite but rather the porosity of the substrate if the resin was not present.

PERMEABILITY Kozeny-Carman relations have long been used to estimate permeability of porous media.[35] Though originally formulated for a bed of packed spheres, Kozeny-Carman has been expanded to other porous media. This methodology uses an extension of Kozeny-Carman to an arbitrary randomly-oriented, three dimensional fiber mat based on diffusion theory.[36] Nondimensional permeability is estimated:

$$\frac{K}{d_{\text{fiber}}^2} = \frac{\phi}{32 \ln^2 \phi} \frac{(\phi - \phi_p)^{\alpha+2}}{(1-\phi_p)^{\alpha} \left[(\alpha+1)\phi - \phi_p\right]^2} \tag{6}$$

where ϕ_p, the percolation threshold, and α are numerically derived quantities dependent on geometry and $\phi_p = 0.037$ and $\alpha = 0.661$ for 3-D randomly overlapped fibrous media. Note the notation has been altered from the original to fit the nomenclature of this paper.

Estimated permeability, plotted as a function of porosity, is presented for several fiber diameters (Figure 4). The lefthand plot depicts permeability across the full range of porosity, while the righthand plot shows a narrower range relevant to the high porosity materials of this work. Note that porosity here is that of the substrate compressed within the mold, ϕ^{pre}, so that K corresponds to the material as infused. Because of the random nature of the fiber network, K is assumed to be equal in all directions.

2. *Resin Solution Properties*

The following properties are quantities for the resin mixture averaged over its components. It is important to note that component properties must be specified at the infusion temperature – typically, room temperature for conformal ablators. Extrapolating to other temperatures may be possible with knowledge of component

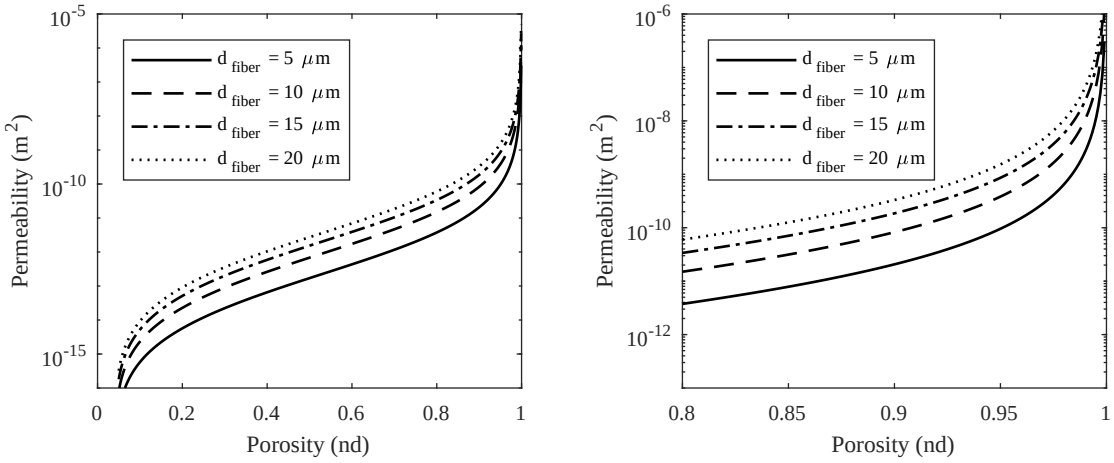

Figure 4. Permeability of a three-dimensional, random fiber network.

properties as functions of temperature. However, an isothermal process is assumed here. Furthermore, an ideal solution is assumed, i.e., interaction between unlike molecules can be neglected and mixture properties are functions of the individual components weighted by their relative proportions.

Dynamic Viscosity This work leverages the Refutas model,[37] originally developed for petroleum blends to approximate kinematic viscosity, ν, of a solution. The Refutas model employs a viscosity blending index (VBI) for each component c of the mixture,

$$\mathrm{VBI}_c = 10.975 + 14.535 \ln\left[\ln\left(\nu_c + 0.8\right)\right] \tag{7}$$

The VBI of the mixture is a weighted sum of the component VBI_c,

$$\mathrm{VBI}_{\mathrm{sol}} = \sum_c w_c \mathrm{VBI}_c \tag{8}$$

where w_c is the weight fraction. Rearranging Equation 7 yields an expression for the kinematic viscosity of the solution as a function of the mixture VBI,

$$\nu_{\mathrm{sol}} = \exp\left[\exp\left(\frac{\mathrm{VBI}_{\mathrm{sol}} - 10.975}{14.535}\right)\right] - 0.8 \tag{9}$$

Finally, dynamic viscosity, $\mu_{\mathrm{sol}} = \nu_{\mathrm{sol}}\rho_{\mathrm{sol}}$, is required for Darcy's law. If not known, resin solution density may be approximated using a weighted average of its components.

Vapor Pressure VIP is highly sensitive to vacuum level during mold filling. Ideally, pressure should be as low as possible to ensure low voidage (around 1 mmHg is recommended[33]). However, if pressure is too low, boiling may occur along the flow front, which may also lead to entrapped gas and voidage. Boiling is of particular concern for conformal ablators due to resin dilution and low vapor pressure. Vapor pressure is estimated using Raoult's law, the sum of component vapor pressures weighted by mole fraction,

$$P_{\mathrm{vap,sol}} = \sum_c P_{\mathrm{vap},c} x_c \tag{10}$$

The process pressure must not fall below the vapor pressure of the solution, or boiling will occur. Thus, for simulation purposes, the vent pressure, P_{vent}, is set equal to $P_{\mathrm{vap,sol}}$. In reality, vapor pressure may deviate from that predicted by Raoult's law due to the suppression or enhancement of intermolecular forces between unlike molecules. Thus, this method provides a first order approximation which can be adjusted as necessary in subsequent processing.

3. Composite Properties

Dimensional Changes during Processing Shrinkage of the resin system during processing changes overall part dimensions. Dimensional changes are broken down into an in plane component, $\left(\frac{\Delta l}{l}\right)_{\text{IP}}$, and a through thickness component, $\left(\frac{\Delta l}{l}\right)_{\text{TT}}$. These quantities can be approximated as functions of the pure resin shrinkage and the substrate porosity, but these details are left to future work. Instead, in the example, these values are drawn from experiment and treated as a priori inputs. Through thickness shrinkage leads to a maximum composite thickness of

$$t_{\text{comp}}^{\max} = (t_{\text{sub}} - \Delta t_{\text{sub}}) \left[1 - \left(\frac{\Delta l}{l}\right)_{\text{TT}}\right] \tag{11}$$

which constrains TPS thickness.

Resin Density in the Composite Resin density in the composite post-processing, $\rho_{\text{resin}}^{\text{post}}$, is coupled to the material shrinkage and functionally depends on the shrinkage and density of the pure resin. That is, a stiff substrate yields little volume contraction, and thus lower resin density, compared to a compliant substrate. $\rho_{\text{resin}}^{\text{post}}$ is averaged over the post-process porous volume. Thus, it is not a measure of the local resin density, which is somewhat higher due to clumping around the fibers, but rather the density if the resin were uniformly distributed throughout the porous volume. As above, the details of this estimation are left to future work with experimentally derived results used here.

C. Tile Layout

Tiling converts an untiled heatshield geometry (the input) into segmented, manufacturable tiles (the output) based on a set of layout rules (constraints). Some constraints are implicitly enforced by the approach described below; other constraints are explicitly applied in the optimization. The optimal design is that with the minimum total number of tiles (the objective function). The goal of this step is to minimize manufacturing time and cost. While these quantities are not directly estimated, they are closely coupled to the number of unique molds / tools and the number of processing runs. In the present approach, each tile requires one VIP run, and each tile geometry requires one tooling set. Minimizing these quantities can limit costs (both non-recurring and recurring) and manufacturing time. In addition, fewer tiles greatly simplifies aeroshell integration – fewer tiles translates to fewer seams and less gap filling.

Tiling proceeds radially outward from the nose of the vehicle forming axisymmetric, concentric rings with orthogonal seams between tiles. The details of the seam geometry itself is not considered here – each tile is assumed to butt up against the next at a perpendicular joint. Each ring is divided into an integer number of identical tiles (thus, each ring requires only one mold to fabricate). Each segment of the OML is treated separately starting with the nose. For example, tiling a biconic aeroshell proceeds from the nose to the first conical segment and then the second conical segment (Figure 5). Tiles do not span these segments. Thus, a seam exists at the boundary between adjacent segments. Each segment is operated upon to generate the optimal tile layout for that segment producing a layout consisting of M OML segments each composed of $Q_i^{\min}$ rings. $Q_i^{\min}$ is the minimum number of rings required to tile segment i and is computed from substrate dimensions.

This work considers OML geometries with circular (nose) and linear (conical flank) segments. Geometry is specified by a radial and height position relative to the vehicle nose, $(r_{i,j}, z_{i,j})$. Subscripts denote segment and ring indices, $i = [1, M]$ and $j = [1, Q_i^{\min}]$, respectively. Segment geometries are defined by start and endpoints: $(r_{i,1},\ z_{i,1})$ and $(r_{i+1,1},\ z_{i+1,1})$. The circular nose segment also includes a center, $(r_{i,1}, z_{i,1})$, and radius of curvature, R_1 (Figure 6). Within each segment, ring j spans from $(r_{i,j}, z_{i,j})$ to $(r_{i,j+1}, z_{i,j+1})$. The nose is formed as a single tile if possible and, thus, its design is trivial. The methodology does not handle nose segments larger than that manufacturable as a single tile. The following discussion describes the optimization procedure applied to the subsequent conical segment(s).

1. Inputs

Inputs to the optimization include TPS geometry (OML segment geometry and desired TPS thickness, t_{TPS}), substrate geometry (W_{sub}, L_{sub}), and processing characteristics ($t_{\text{comp}}^{\max}$, maximum processed material thickness and $\left(\frac{\Delta l}{l}\right)_{\text{IP}}$, in plane shrinkage). Finally, the minimum radius of curvature, $R^{\min}$, and minimum seam angle, $\beta^{\min}$, are required to enforce their respective constraints.

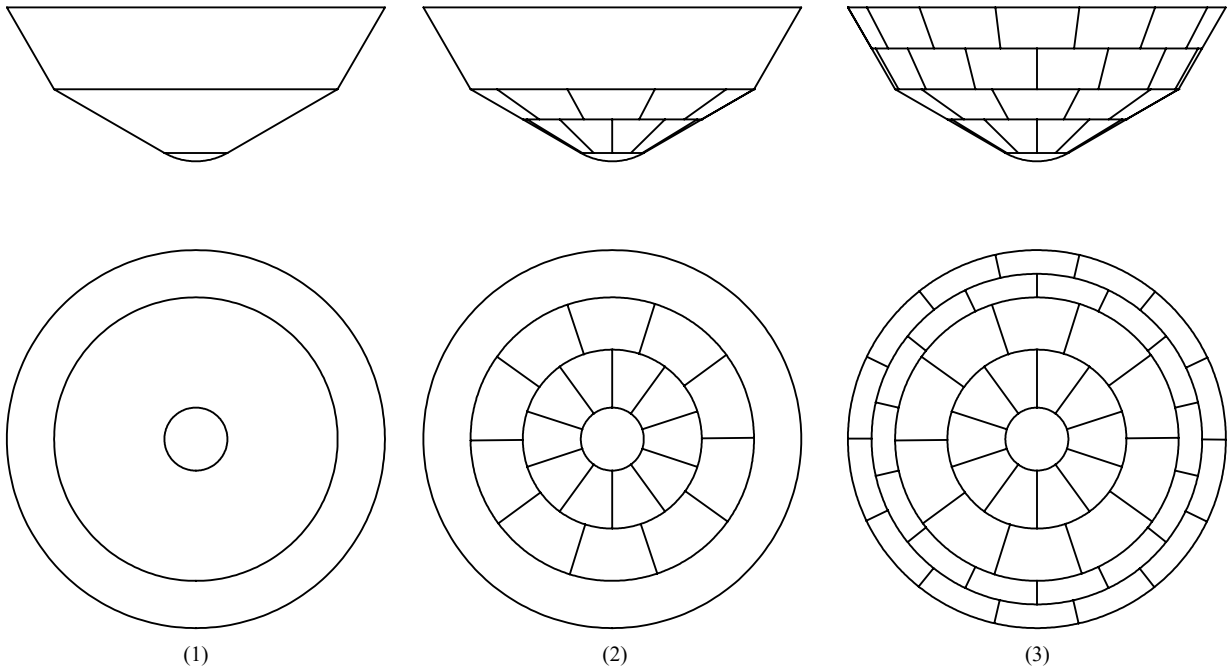

Figure 5. Approach to generating tile layout for a biconic aeroshell: (1) nose tile, (2) 1st conical flank, and (3) 2nd conical flank.

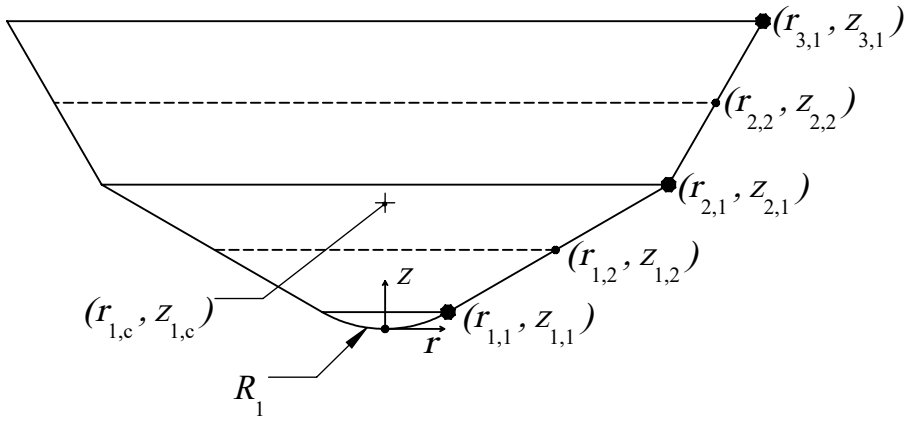

Figure 6. An example OML geometry illustrating geometry definitions.

2. Optimization

Independent Variables The independent design variables are the numbers of tiles in each concentric ring. Moving from the innermost to the outermost ring, these are denoted by N_j, $j = [1, Q_i]$.

Dependent Variables Dependent variables, computed quantities following from the design specification, include the dimensions of the curved tile as installed on the heatshield, the dimensions of the curved substrate, and the dimensions of the corresponding substrate once flattened. For example, the angle the curved tile spans on the heatshield, $\gamma_j = 2\pi/N_j$, is scaled up to a corresponding angle spanned by the substrate, γ_j^{sub}, and then transformed to a flat pattern angle, γ_j^f. Other parameters are similarly transformed (Figure 7). Note that these transformations are functionally dependent on segment geometry as well as the in plane material shrinkage during processing. A sub-optimizer maximizes substrate side length l_j^{sub} given γ_j^f and $r_{i,j}^f$ and subject to substrate dimensions. Maximum substrate length is then transformed back to a maximum tile length, $l_j^{\max}$, scaling by the shrinkage. $l_j^{\max}$ is connected to the OML geometry through $l_j^{\max} = \sqrt{(r_{i,j+1} - r_{i,j})^2 + (z_{i,j+1} - z_{i,j})^2}$. Thus, the starting coordinate of each ring depends on that of the preceding one. In this way, tile layout is built radially outward.

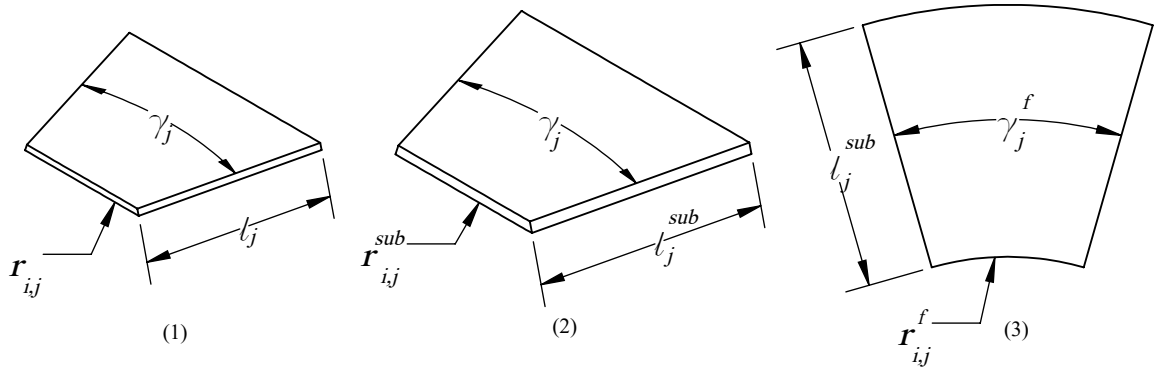

Figure 7. Transformation of tile geometry (left) to scaled up substrate geometry (center) and, finally, to two-dimensional flat pattern (right).

Objective Function The objective function minimized by the optimization routine is simply the sum of all N_j,

$$f_{\text{obj},1} = \sum_{j=1}^{Q_i^{\min}} N_j \tag{12}$$

Constraints The layout is subject to several constraints (Table 1) that ensure the design is manufacturable within size and curvature limitations and that seams of adjacent rings do not align. Manufacturing constraints are applied, first, by two inequalities: $t_{\text{TPS}} \leq t_{\text{comp}}^{\max}$ and $r_{i,j}^{\text{sub}} \geq R^{\min}$, $j = [1, Q_i^{\min}]$. The first inequality ensures that TPS thickness is not larger than that of the processed material. If this constraint is violated, the methodology terminates as no design would be feasible. Either the TPS thickness must be adjusted or another substrate must be selected. The second inequality enforces the limit on curvature. This inequality compares the minimum radius of curvature for each tile to the material constraint. If this second inequality is violated, the infringing tile(s) is (are) flagged, but the optimization continues. Flagging warns the designer that this tile geometry may present a challenge for VIP due to substrate wrinkling. An alternate design, material, or process may be required in these cases to avoid wrinkling. To ensure the set of N_j can fully span the OML segment, the sum of all $l_j^{\max}$ must be greater than or equal to the total segment length, $\sqrt{(r_{i+1,1} - r_{i,1})^2 + (z_{i+1,1} - z_{i,1})^2}$. The minimum seam angle, $\beta_{\min}$, prevents radial seams of adjacent rings from being aligned. The methodology computes the minimum seam angle between adjacent rings j and $j+1$,

$\beta^{\min}_{j,j+1}$. All $\beta^{\min}_{j,j+1}$ must be larger than the minimum, or the design is infeasible. Finally, side constraints are imposed on the N_j to practically limit the design space.

Table 1. Summary of tiling constraints for OML segment i.

Description	Variable(s)	Type of Constraint	Constraint
Thickness	t_{TPS}	Inequality	$t_{\text{TPS}} \leq t^{\max}_{\text{comp}}$
Radius of Curvature	R_i, $r_{i,j}$	Inequality	$r^{\text{sub}}_{i,j} \geq R^{\min}$, $j = [1, Q^{\min}_i]$
Segment Length	$l^{\max}_j$	Inequality	$\sum_{j=1}^{Q^{\min}_i} l^{\max}_j \geq \sqrt{(r_{i+1,1} - r_{i,1})^2 + (z_{i+1,1} - z_{i,1})^2}$
Seam Angle	$\beta_{j,j+1}$	Inequality	$\beta^{\min}_{j,j+1} \geq \beta_{\min}$, $j = [1, Q^{\min}_i - 1]$
Number of Tiles in a Ring	N_j	Side	$N_{\text{lb}} \leq N_j \leq N_{\text{ub}}$

3. *Outputs*

Two outputs follow from the tiling procedure described above – the set of unique tile geometries and the corresponding substrate geometries required to make them. That is, for a tile layout design comprised of Q rings, there are Q tile geometries and Q substrate geometries. Recall that the substrate is scaled up from the final tile geometry to account for process shrinkage. Futhermore, the substrate geometries yielded by the procedure consist of both the two-dimensional flat pattern, used for cutting the substrate from the raw material, and the three-dimensional curved geometry, used in simulating the infusion process. The latter output is the subject of the next step outlined below.

D. Mold and Process Design

The next step of the methodology takes the optimal set of tile geometries, with the corresponding substrate geometries, generated above and simulates mold filling to produce an optimal mold design for each tile. Mold filling is simulated on the curved substrate geometry as it is draped in the mold. Designs are limited to single gate, single vent configurations as mentioned earlier. Gate location is varied to reach an optimal position. Generally speaking, the "best" designs are those that prevent voids from air entrapment during infusion. The objective function quantifying optimality is discussed below. Leveraging the fact that TPS tiles are typically much smaller through the thickness than in plane, infusion is simulated on a two-dimensional shell to speed iteration. This neglects through the thickness variation in substrate properties due to draping, but these variations are typically small for the materials and geometries here.

Before discussing the optimization procedure itself, it is instructive to provide some background on the mold filling simulation. Mold filling is simulated in Liquid Injection Molding Simulation (LIMS), a finite element/control volume (CV/FE) simulation developed at University of Delaware.[38] The CV/FE approach to mold filling is a widely used computational technique first developed by Bruschke and Advani.[12] It leverages the computational efficiency of a fixed finite element mesh while obeying local conservation of mass. The simulation uses a two step solution process applied repeatedly until the mold is completely filled – (1) solving for the pressure field in the saturated region using the governing equation, then (2) updating the location of the saturated region (the flow front) by applying Darcy's law. The latter is achieved by tracking fluid flow into and out of control volumes (CV) around each mesh node. A fill factor, f, denotes the fraction of resin saturation within a CV allowing numerical representation of an empty node, $f = 0$, a fully saturated node, $f = 1$, and a partially saturated node, $0 < f < 1$. Logically, partially saturated nodes represent the approximate flow front location. This work is primarily concerned with flow front location as a function of time along the perimeter of the part, which yields an indication of air entrapment during processing.

1. *Inputs*

Inputs to the mold and process design steps include substrate geometry, material properties, and process settings. As described above, substrate geometry is that of the three-dimensional, curved material and is scaled up from the tile geometry to account for process shrinkage. Material properties include the porosity and permeability of the substrate, and the dynamic viscosity of the resin – the parameters appearing in Darcy's law (Eq. 2). Note that substrate quantities are for the material compressed in the mold. Thus, these are the pre-process quantities of the substrate: ϕ^{pre} and its corresponding K.

The final inputs form the boundary conditions for mold filling. These parameters are the gate design and the vent pressure. This work uses a circular, constant pressure gate with fixed radius, R_{gate}. Gate pressure is atmospheric pressure minus vent pressure, P_{vent}, where vent pressure is set to the vapor pressure of the resin solution.

2. *Optimization*

INDEPENDENT VARIABLES Independent design variables describe the position of the gate relative to the curved substrate geometry: non-dimensional radial, λ_{gate}, and angular, Γ_{gate}, locations defined as fractions of substrate length, l_j^{sub}, and angular span, γ_j^{sub},

$$\lambda_{\text{gate}} = \frac{l_{\text{gate}}}{l_j^{\text{sub}}} \tag{13}$$

$$\Gamma_{\text{gate}} = \frac{\gamma_{\text{gate}}}{\gamma_j^{\text{sub}}} \tag{14}$$

where both quantities can range from [0,1]. Note that the vent is implicitly assumed to be located at the last point reached by the flow. Thus, vent location is not controlled by the optimization but is instead dependent on the other simulation parameters.

MESH GENERATION Two-dimensional finite element meshes are automatically generated in gmsh using meshing rules generalized to an arbitrary tile geometry and gate location. Element sizes scale proportionally with tile size maintaining an approximately constant number of elements. Elements are concentrated near the gate to capture rapid flow advancement in that region. Similarly, elements are concentrated around the perimeter of the part to capture flow front detail in that region. An example mesh generated using these element spacing rules is depicted in Figure 8.

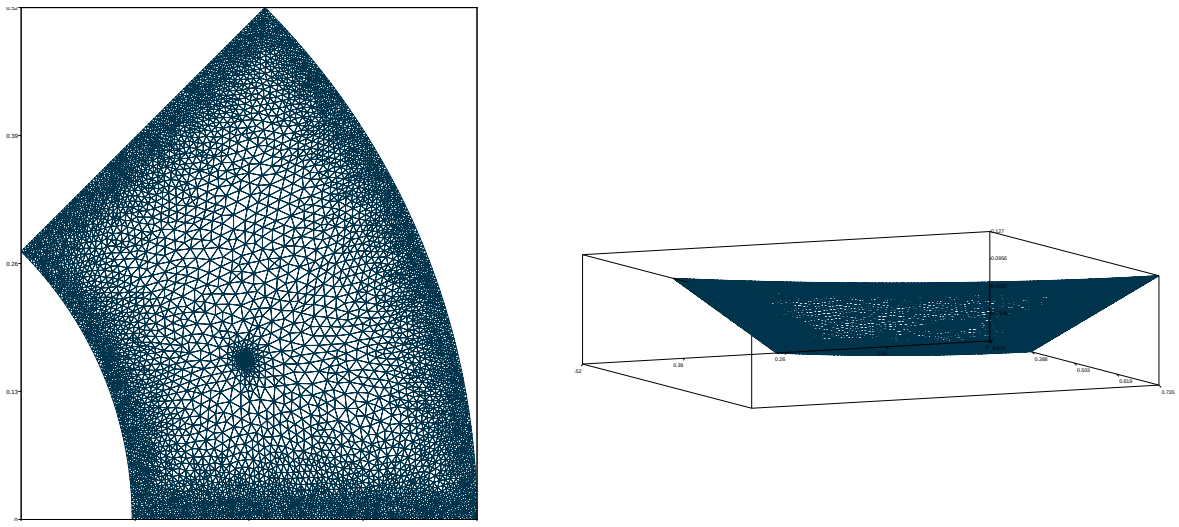

Figure 8. An example two-dimensional finite element mesh used to simulate mold filling.

OBJECTIVE FUNCTION Each mold design is evaluated according to the objective function,

$$f_{\text{obj},2} = \frac{p'}{p_{\text{total}}} \tag{15}$$

where p' is the length of the perimeter blocked from the vent during processing and p_{total} is the total perimeter length. Thus, $f_{\text{obj},2}$ ranges from [0,1] and reflects the proportion of the perimeter that is blocked (i.e., unfilled with no path for air to escape through the vent). Practically, $f_{\text{obj},2}$ quantifies the degree of air entrapment during infusion, which can lead to incomplete infusion and voidage. Minimizing $f_{\text{obj},2}$ limits this risk, ensuring complete saturation of the substrate. p' is computed by simulating mold filling on the

specified design and extracting the time to fill for nodes along the perimeter. This yields the time to fill as a function of distance along the perimeter, $T_f(p)$, which is operated upon to compute p' (Figure 9). Note that two curves are plotted, one for each direction around the perimeter. Each curve begins and ends at the same location and time – the first and the last point reached by the flow, respectively. p' is computed by summing the length of blocked regions. These regions correspond to two perimeter points with the same time to fill $T_f(p_2) = T_f(p_1)$, where $p_2 > p_1$. That is, the flow front has reached two different locations on the perimeter at the same time. The length of blocked region k is $p'_k = p_2 - p_1$ and summing over all blocked regions gives the total blocked length $p' = \sum_k p'_k$.

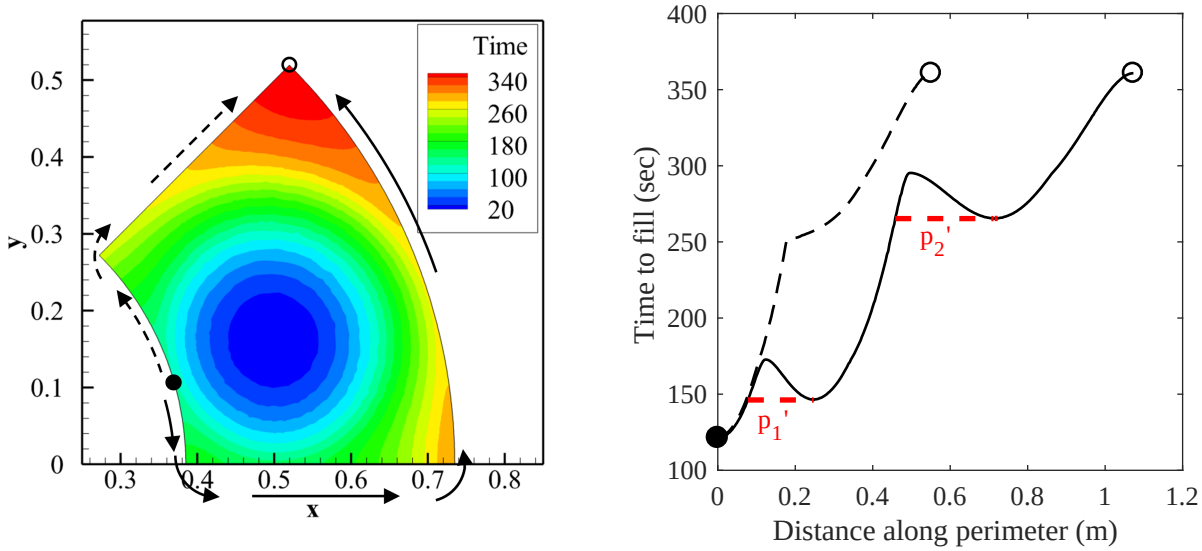

Figure 9. Simulation results showing time to fill across the part (left) and those results extracted along the perimeter to yield time to fill as a function of perimeter location (right).

CONSTRAINTS Gate location is constrained so that it falls within the two-dimensional footprint of the tile. A keepout area offset by R_{gate} from the perimeter enforces this requirement. The mathematical constraints are summarized in Table 2. Note that the upper bound on Γ_{gate} leverages the fact that tiles are symmetric down the midline and thus only one half of the tile need be considered. Angular position is generated such that $\Gamma = 0$ corresponds to a gate tangent to the side of the tile.

Table 2. Constraints on mold design.

Description	Variable(s)	Type of Constraint	Constraint
Radial position	λ_{gate}	Side	$\frac{R_{\text{gate}}}{l_j^{\text{sub}}} < \lambda_{\text{gate}} < 1 - \frac{R_{\text{gate}}}{l_j^{\text{sub}}}$
Angular position	Γ_{gate}	Side	$0 \leq \Gamma_{\text{gate}} \leq 0.5$

3. Outputs

Iteration on the mold filling simulation yields optimal gate and vent locations for the given geometry, material and process parameters. These locations inform subsequent tooling design. Additional results from this step include vent pressure, total mold filling time, and resin consumption. With a selected gate position, mold filling is simulated on the full three-dimensional geometry (with finite thickness) to obtain accurate filling time and resin consumption. These parameters are important both for the designer and for those processing the material. For example, knowing mold filling time helps a process technician anticipate when flow must be shut off, and vent pressure indicates the correct setting for the vacuum pump during processing. From a broader perspective, mold filling time and resin consumption impact the overall process timeline and cost.

Relevant properties of the fabricated TPS material are also important outputs for the designer, and these quantities are the subject of the last part of the methodology.

E. TPS Material Property Estimation

In the final step, selected properties of the fabricated composite TPS material (virgin density, ρ_{comp}; char yield, Y_{comp} and resin mass fraction, w_{resin}) are computed. Employing the filamentary analog model discussed earlier simplifies substrate properties to closed form functions of known, or previously computed, densities. Resulting expressions for TPS properties are summarized in Table 3. Post-process porosity is reproduced here for simplicity (Equation 5). A detailed discussion of their derivation is found in related work.[11] Though not presented here, these expression can be used to estimate uncertainties as well.

Table 3. Expressions for estimating properties of the final TPS / composite material.

Property	Symbol	Model
Porosity	ϕ^{post}	$\left(1 - \frac{\rho_{\text{sub}}^{\text{post}}}{\rho_{\text{fiber}}}\right)$
Virgin density	ρ_{comp}	$\rho_{\text{sub}}^{\text{post}} + \rho_{\text{resin}}^{\text{post}}\phi^{\text{post}}$
Char yield	Y_{comp}	$\frac{\rho_{\text{sub}}^{\text{post}} + Y_{\text{resin}}\rho_{\text{resin}}^{\text{post}}\phi^{\text{post}}}{\rho_{\text{comp}}}$
Resin mass fraction	w_{resin}	$\frac{\rho_{\text{resin}}^{\text{post}}\phi^{\text{post}}}{\rho_{\text{comp}}}$

IV. Results

Results of the methodology are presented for an example heatshield based on the MSL forebody aeroshell, a 4.5 meter diameter, 70 degree sphere-cone. The TPS material is loosely based on an existing C-PICA formulation comprised of a rayon-based carbon felt (Morgan Advanced Materials VDG Carbon Felt) and a proprietary phenolic resin solution. The felt has nominal bulk density of 0.09 g/cc and a nominal thickness of 0.88 in. In practice, the thickness varies from 0.80 – 0.96 in, so $\Delta t_{\text{sub}} = 0.08$ in. Resin loading is approximately 0.2 g/cc resulting in a TPS density of around 0.29 g/cc. TPS thickness is set to $t_{\text{TPS}} = 0.75$ in to meet manufacturing constraints for the given substrate. Substrate size is 1 meter by 1 meter. In plane shrinkage is 1% during processing while the through thickness shrinkage is 5% reflecting typical results.[11] Some quantities for the resin have been changed due to its proprietary nature. Resin char yield data was obtained from Milos, et al.[5] Post-process resin density is drawn from experimental results for VIP-fabricated C-PICA ($\rho_{\text{resin}}^{\text{post}} = 0.188$ g/cc). Results are generated for the nose and conical flank only, neglecting shoulder tiles. Other parameters for the design, a priori inputs and computed quantities, are summarized in Tables 4 and 5, respectively. Finally, constraints on the design are indicated in Table 6.

A. Tile Layout

The optimal tile design consists of a single nose tile, and a flank formed from two rings of 15 tiles each ($N_1 = 1$, $N_2 = 15$, and $N_3 = 15$). The design space for the nose is trivial – the nose is small enough to be fabricated from a single piece of the substrate material. The design space for the conical segment is depicted in Figure 10 (left) with N_3 plotted against N_2. Feasible designs are plotted with the optimal design highlighted. Note that the feasible space is bounded on the left and the bottom by, respectively, $N_2 = 6$ and $N_3 = 14$. That is, no design spans the conical segment if either N_2 or N_3 falls below its respective bounding value. Note also that the minimum seam angle constraint substantially reduces the number of feasible designs, and these designs tend to fall along lines where N_2 and N_3 are integer multiples of one another (e.g., $N_2 = N_3$, $N_2 = 2N_3$, etc.). The optimal layout, the minimum number of tiles, for the conical flank occurs with $N_2 = 15$ and $N_3 = 15$ (Figure 10, right). This layout, and the corresponding substrate geometries (three, in total), are passed to the next step for mold and process design.

B. Mold and Process Design

Figures 11 – 13 depict mold design results for each of the three tile geometries. Each case includes a contour plot of objective function, $f_{\text{obj},2}$, across the design space (left) and simulation results for the optimal design

Table 4. Primary inputs for the example design.

Category	Parameter	Value	Units
Substrate	W_{sub}	1.0	m
	L_{sub}	1.0	m
	t_{sub}	0.88	in
	Δt_{sub}	0.08	in
	ρ_{sub}	0.09	g/cc
	ρ_{fiber}	1.4	g/cc
	d_{fiber}	15	μm
Resin	$\rho_{\text{resin}}^{\text{post}}$	0.188	g/cc
	Y_{resin}	45.9	%
Composite	$\left(\frac{\Delta l}{l}\right)_{\text{TT}}$	0.05	m/m
	$\left(\frac{\Delta l}{l}\right)_{\text{IP}}$	0.01	m/m
Process	R_{gate}	0.125	in
	p_{atm}	101325	Pa

Table 5. Secondary quantities computed for the example design.

Category	Parameter	Value	Units
Substrate	$\rho_{\text{sub}}^{\text{pre}}$	0.099	g/cc
	ϕ^{pre}	0.93	non-dimensional
	K	4.1×10^{-10}	m^2
Resin	μ	100	cP
	p_{vent}	4000	Pa

Table 6. Summary of design constraints for the example.

Description	Variable(s)	Value	Units
Maximum TPS Thickness	$t_{\text{comp}}^{\max}$	0.75	in
Minimum Radius of Curvature	$R^{\min}$	0.15	m
Minimum Seam Angle	$\beta^{\min}$	3	deg
Minimum Number of Tiles in Ring	N_{lb}	2	non-dimensional
Maximum Number of Tiles in Ring	N_{ub}	60	non-dimensional

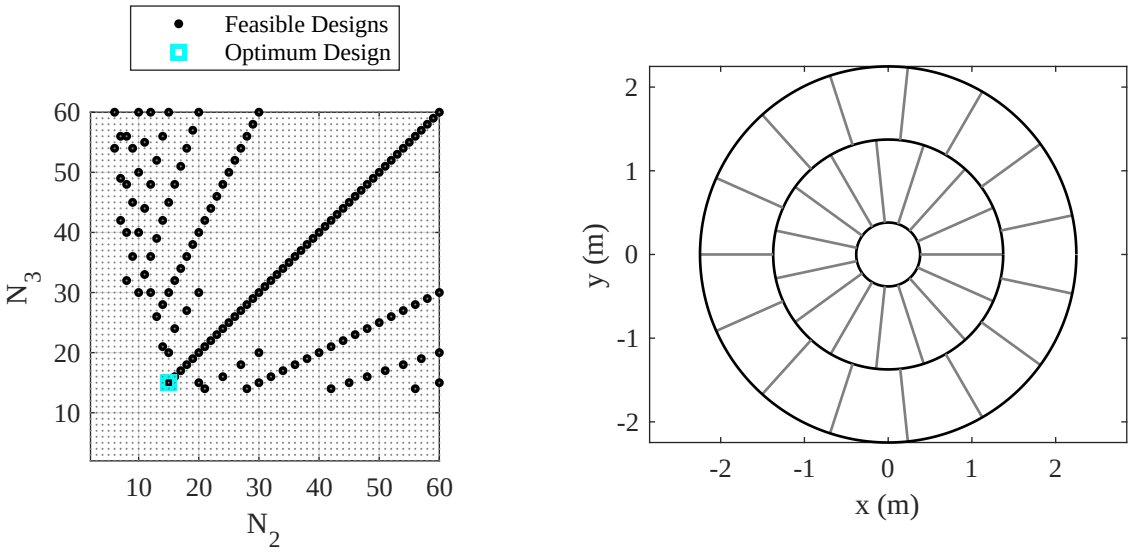

Figure 10. Tile layout design space for the example heatshield (left) and front view of the optimal tile layout with $N_1 = 1$, $N_2 = 15$, and $N_3 = 15$ (right).

(right). Due to symmetry, only λ_{gate} is varied for the nose tile, and there is no dependence on Γ_{gate} (Figure 11, left). In this case, λ_{gate} is defined as a fraction of arc length, from the stagnation point ($\lambda_{\text{gate}} = 0$) to the outer radius ($\lambda_{\text{gate}} = 1$). Simulation results depict time to fill across each tile, ranging from dark blue to dark red. Thus, contours denote flow position over time. Optimal gate and vent locations are highlighted. In all cases, the vent is placed at the last point to be filled. Flow expands outward from the gate and advances toward the vent.

The worst designs, with the highest blocked length, occur with gate location near the center of the tile ($\lambda_{\text{gate}} = 0.5$, $\Gamma_{\text{gate}} = 0.5$). In these designs, large regions of the mold (greater than half the perimeter) are cut off from the vent by advancing flow and have a high likelihood of air entrapment. Objective function decreases as gate placement shifts away from the central region of the part, indicating smaller blocked length and lower risk of air entrapment.

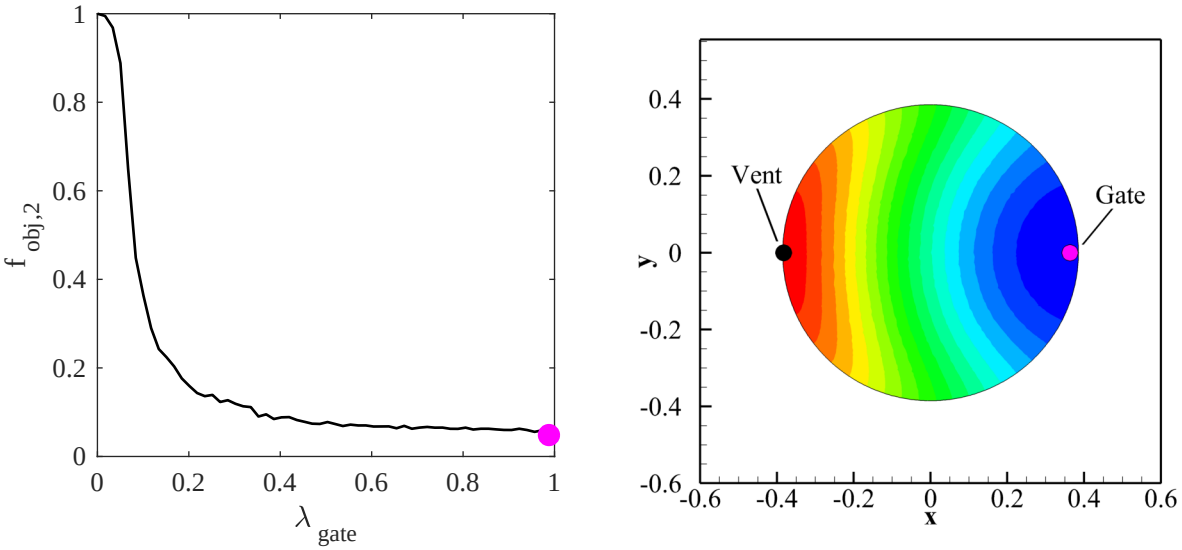

Figure 11. Mold design results for nose tile: design space with optimal design highlighted (left) and simulation results using the optimal gate location (right).

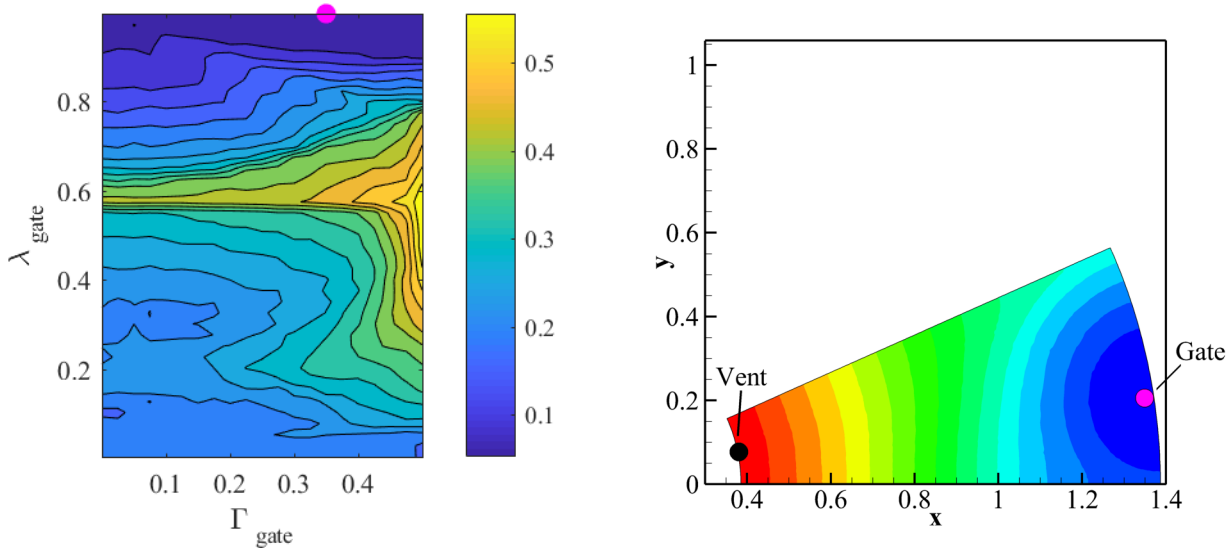

Figure 12. Mold design results for inner ring of conical flank: design space with optimal design highlighted (left) and simulation results using the optimal gate location (right).

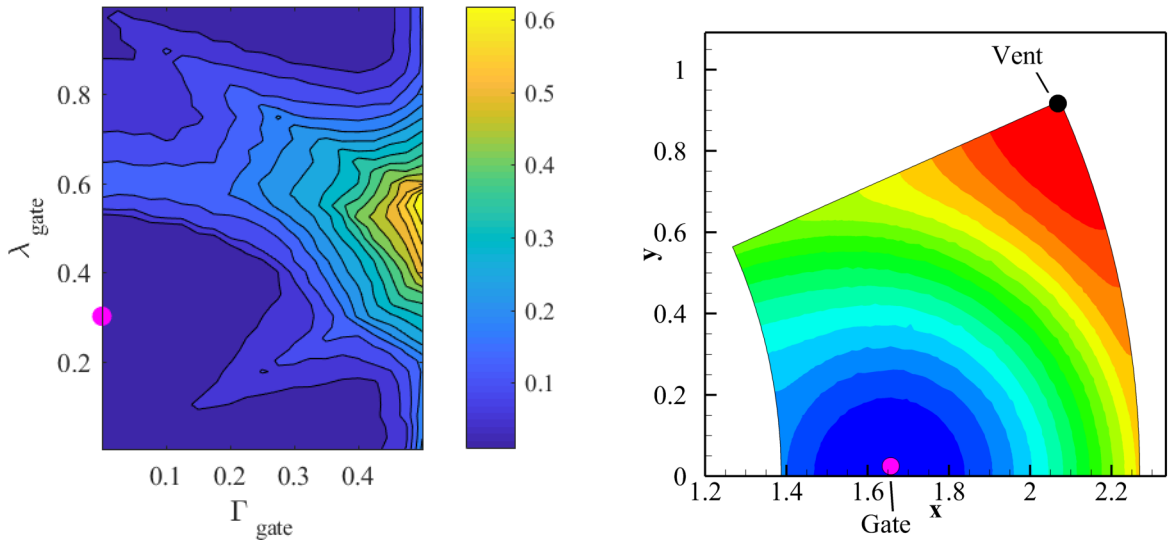

Figure 13. Mold design results for outer ring of conical flank: design space with optimal design highlighted (left) and simulation results using the optimal gate location (right).

For the nose tile (Figure 11), the value of the objective function quickly decreases as gate location moves from the center to the outer radius, approaching $f_{\text{obj},2} = 0$. This result is logical for the given geometry – the flow front is circular for an isotropic material. Thus, for a centrally located gate, $\lambda_{\text{gate}} = 0$, the front reaches every point on the perimeter at the same time and $f_{\text{obj},2} = 1$. Any off center position, $\lambda_{\text{gate}} > 0$, produces a flow front that arrives at the perimeter at a single point and progresses monotonically with time yielding $f_{\text{obj},2} = 0$. In theory, then, gate location could be anywhere other than $\lambda_{\text{gate}} = 0$. However, flow front arrival at the perimeter occurs at very nearly the same time for gates close to the center of the part. Therefore, in actual processing where substrate variability results in a non-circular flow front, local air entrapment can still occur. A small tolerance introduced into the calculation of the blocked length, p', captures these perimeter regions with similar time to fill. Thus, gate locations near the outer edge are preferred with optimum occurring at $\lambda_{\text{gate}} = 0.99$.

For the inner ring tile (Figure 12), the best designs are at large λ_{gate}, i.e. with the gate located on the outer radius of the tile. The optimum, $f_{obj,2} = 0.05$, occurs at $\lambda_{gate} = 1$, $\Gamma_{gate} = 0.35$. Blocked length is non-negligible (5%) even at the optimum due to the flow front arriving at the inner radial edge at nearly the same time. Nonetheless, the overall blocked volume is small and should not pose a problem in processing.

For the outer ring tile (Figure 13), the best designs occurs with the gate located along the outer radius and in regions near one of the inner corners. Blocked length is smaller for this tile geometry: $f_{obj,2} = 0.01$ across a broad range of gate positions. The optimal location is along the tile side ($\lambda_{gate} = 0.30$, $\Gamma_{gate} = 0$). In this location, the flow front advances along the perimeter nearly monotonically with flow converging to a single point at the vent.

Finally, additional outputs for the optimal designs, time to fill and resin consumption, are summarized in Table 7. Simulations were run on a full three-dimensional mesh to obtain accurate results. Totals are for all tiles on the heatshield. Cumulative infusion time is 1607 min with resin consumption of 0.33 m^3. Note that infusion time could be reduced by pressurizing the resin above atmospheric pressure.

Table 7. Summary of design processing parameters for each tile.

Parameter	Units	Nose Tile	Inner Ring Tile	Outer Ring Tile	Total (all tiles)
Time to Fill	min	32	39	66	1607
Resin Consumption	m^3	9.1 $\times 10^{-3}$	7.5 $\times 10^{-3}$	13.6 $\times 10^{-3}$	0.33

C. TPS Material Property Estimation

Estimated TPS properties agree closely with reference values for C-PICA (Table 8). The post-process substrate density is included for comparison. Deviations from the reference material can be attributed to this difference in substrate density. Substrates are more compressed in the VIP process leading to higher fiber fraction in the final material. In this case, substrate density is predicted to be about 15% higher for the VIP-produced material. Higher fiber fraction yields lower resin loading leading to the observed results: 3% higher virgin density, 3% higher char yield, and 6% lower resin mass fraction. Note that if the substrate density were made equivalent to that of the reference, predicted values match almost exactly.

Table 8. Estimated final TPS properties compared to reference values.

Property	Units	Predicted	Reference**
Post-process substrate density	g/cc	0.106	0.092
Virgin density	g/cc	0.280	0.273
Char yield (composite)	%	66.4	64.2
Resin mass fraction	non-dimensional	0.62	0.66

**Material model parameters for C-PICA.[5]

V. Conclusion

Vacuum infusion processing improves on conformal ablator fabrication by reducing waste and labor and by allowing numerical process simulation. Coupling tile layout with a Darcy's Law mold filling simulation and material property estimation results in a powerful methodology for heatshield design. Optimization tailors tile layout to a given material and generates mold designs to ensure high quality TPS free from macroscopic voidage. The methodology improves on a largely manual current approach to TPS manufacturing design. Automating these aspects of the design frees the designer to consider higher level trades such as alternative material formulations and modified process parameters. Resulting impact on the manufacturing and the final TPS properties are easily and rapidly assessed.

Using this methdology, a design was generated for a 4.5 meter, 70 degree sphere-cone conformal PICA heatshield. The optimal tile layout consisted of a single nose tile and two rings of 15 tiles along the flank. This design meets both substrate size limitations and seam angle constraints while minimizing the total number of tiles. Optimal mold designs minimized blocked length. Preferred gate locations generally occurred along

one or more of the edges of the part. Locations near the center led to a large amount of blockage. Estimated properties of the final TPS showed good agreement with reference values. A slightly higher density material was predicted due to higher compression for the vacuum infusion process.

Acknowledgments

This work was supported through a NASA Space Technology Research Fellowship, Grant #NNX14AL53H. The authors would like to thank Robin A.S. Beck and Margaret M. Stackpoole, both of NASA Ames Research Center, for their support and guidance on this work.

References

[1]Beck, R. A. S., Gasch, M. J., and Calomino, A., "An overview of NASA's current materials development efforts for Mars EDL," *8th International Planetary Probe Workshop*, Portsmouth, VA, 2011.

[2]Arnold, J. O., Venkatapathy, E., and Beck, R. A. S., "Flexible Ablators: Applications and Arcjet Testing," *8th International Planetary Probe Workshop*, Portsmouth, VA, 2011.

[3]Beck, R. A. S., Arnold, J. O., Gasch, M. J., Stackpoole, M., Prabhu, D., Szalai, C. E., Wercinski, P., and Venkatapathy, E., "Conformal Ablative Thermal Protection System for Planetary and Human Exploration Missions: An Overview of the Technology Maturation Effort," *10th International Planetary Probe Workshop*, San Jose, CA, 2013.

[4]Gasch, M., Agrawal, P., and Beck, R., "Testing of Advanced Conformal Ablative TPS," *10th International Planetary Probe Workshop*, San Jose, CA, 2013.

[5]Milos, F. S., Gasch, M. J., and Prabhu, D. K., "Conformal Phenolic Impregnated Carbon Ablator Arcjet Testing, Ablation, and Thermal Response," *Journal of Spacecraft and Rockets*, Vol. 52, No. 3, 2015, pp. 804–812.

[6]Venkatapathy, E., Feldman, J., Beck, R., Gage, P., Wercinski, P., Ellerby, D., and Munk, M., "Development Challenges of Game-Changing Entry System Technologies From Concept to Mission Infusion," *IEEE Aerospace Sciences*, Big Sky, MT, 2016.

[7]Gasch, M., Stackpoole, M., White, S., and Boghozian, T., "Development of Advanced Conformal Ablative TPS Fabricated from Rayon- and Pan-Based Carbon Felts," *57th AIAA/ASCE/AHS/ASC Structures, Structural Dynamics, and Materials Conference*, American Institute of Aeronautics and Astronautics, Reston, Virginia, 2016.

[8]Beck, R. A. S., Arnold, J. O., Gasch, M. J., Stackpoole, M., Wercinski, P., Venkatapathy, E., Fan, W., Thornton, J., and Szalai, C. E., "Conformal Ablative Thermal Protection System for Planetary and Human Exploration Missions," *9th International Planetary Probe Workshop*, Toulouse, France, 2012.

[9]Beck, R. A. S., Arnold, J. O., Gasch, M. J., Stackpoole, M., and Venkatapathy, E., "Development of a Conformal Ablative Backshell Thermal Protection System for Outer Planetary Exploration Missions," *Outer Planets Assessment Group*, No. July, Bethesda, MD, 2014.

[10]Beck, R., Gasch, M., Stackpoole, M., Wilder, M., Boghozian, T., Prabhu, D., Kazemba, C., and Venkatapathy, E., "Conformal Ablative Thermal Protection Systems (CA-TPS) for Venus and Saturn Backshells," *Outer Planets Advisory Group*, 2016.

[11]Sidor, A. T., Braun, R. D., Beck, R. A., and Stackpoole, M. M., "Vacuum Infusion Process Development for Conformal Ablative Thermal Protection System Materials," *AIAA Space Conference & Exposition*, Orlando, FL, 2017.

[12]Bruschke, M. V. and Advani, S. G., "A finite element/control volume approach to mold filling in anisotropic porous media," *Polymer Composites*, Vol. 11, No. 6, 1990, pp. 398–405.

[13]Wright, M. J., Hughes, M., Calomino, A., and Barnhardt, M. D., "An Overview of Technology Investments in the NASA Entry Systems Modeling Project," *53rd AIAA Aerospace Sciences Meeting*, Kissimmee, FL, 2015.

[14]Chan, A. W. and Hwang, S.-T., "Modeling of the impregnation process during resin transfer molding," *Polymer Engineering and Science*, Vol. 31, No. 15, 1991, pp. 1149–1156.

[15]Correia, N. C., Robitaille, F., Long, A. C., Rudd, C. D., Simacek, P., and Advani, S. G., "Use of Resin Transfer Molding Simulation to Predict Flow, Saturation, and Compaction in the VARTM Process," *Journal of Fluids Engineering*, Vol. 126, No. 2, 2004, pp. 210–215.

[16]Correia, N., Robitaille, F., Long, A., Rudd, C., Simacek, P., and Advani, S., "Analysis of the vacuum infusion moulding process: I. Analytical formulation," *Composites Part A: Applied Science and Manufacturing*, Vol. 36, No. 12, dec 2005, pp. 1645–1656.

[17]Han, K., Jiang, S., Zhang, C., and Wang, B., "Flow modeling and simulation of SCRIMP for composites manufacturing," *Composites Part A: Applied Science and Manufacturing*, Vol. 31, No. 1, 2000, pp. 79–86.

[18]Jiang, S., Zhang, C., and Wang, B., "Optimum arrangement of gate and vent locations for RTM process design using a mesh distance-based approach," *Composites Part A: Applied Science and Manufacturing*, Vol. 33, No. 4, apr 2002, pp. 471–481.

[19]Gokce, A., Hsiao, K.-T., and Advani, S. G., "Branch and bound search to optimize injection gate locations in liquid composite molding processes," *Composites Part A: Applied Science and Manufacturing*, Vol. 33, No. 9, sep 2002, pp. 1263–1272.

[20]Mathur, R., Advani, S. G., and Fink, B. K., "Use of genetic algorithms to optimize gate and vent locations for the resin transfer molding process," *Polymer Composites*, Vol. 20, No. 2, apr 1999, pp. 167–178.

[21]Ruiz, E., Achim, V., Soukane, S., Trochu, F., and Bréard, J., "Optimization of injection flow rate to minimize micro/macro-voids formation in resin transfer molded composites," *Composites Science and Technology*, Vol. 66, No. 3, 2006, pp. 475–486.

[22]Liu, B., Bickerton, S., and Advani, S. G., "Modelling and simulation of resin transfer moulding (RTM) - Gate control, venting and dry spot prediction," *Composites Part A: Applied Science and Manufacturing*, Vol. 27, No. 2, 1996, pp. 135–141.

[23]Todd, D. K. and Mays, L. W., *Groundwater Hydrology*, Wiley, 3rd ed., 2004.

[24]Pierson, H. O., "Graphite Structure and Properties," *Handbook of Carbon, Graphite, Diamonds and Fullerenes*, Elsevier, 1993, pp. 43–69.

[25]Morgan, P., "Properties of Carbon Fibers," *Carbon Fibers and Their Composites*, chap. 20, CRC Press, Boca Raton, FL, 2005, pp. 791–859.

[26]Panerai, F., Ferguson, J. C., Lachaud, J., Martin, A., Gasch, M. J., and Mansour, N. N., "Micro-tomography based analysis of thermal conductivity, diffusivity and oxidation behavior of rigid and flexible fibrous insulators," *International Journal of Heat and Mass Transfer*, Vol. 108, 2017, pp. 801–811.

[27]Prodromou, A. and Chen, J., "On the relationship between shear angle and wrinkling of textile composite preforms," *Composites Part A: Applied Science and Manufacturing*, Vol. 28, No. 5, jan 1997, pp. 491–503.

[28]Bickerton, S., Sozer, E., Šimácek, P., and Advani, S., "Fabric structure and mold curvature effects on preform permeability and mold filling in the RTM process. Part II. Predictions and comparisons with experiments," *Composites Part A: Applied Science and Manufacturing*, Vol. 31, No. 5, 2000, pp. 439–458.

[29]Williams, S. D. and Curry, D. M., "Thermal protection materials: Thermophysical property data," Tech. rep., National Aeronautics and Space Administration, 1992.

[30]Parker, J. A. and Winkler, E. L., "The effects of molecular structure on the thermochemical properties of phenolics and related polymers," Tech. rep., 1967.

[31]Wang, Y., Wang, S., Bian, C., Zhong, Y., and Jing, X., "Effect of chemical structure and cross-link density on the heat resistance of phenolic resin," *Polymer Degradation and Stability*, Vol. 111, 2015, pp. 239–246.

[32]Friedman, H. L., "Kinetics of thermal degradation of char-forming plastics from thermogravimetry. Application to a phenolic plastic," *Journal of Polymer Science Part C: Polymer Symposia*, Vol. 6, No. 1, 1964, pp. 183–195.

[33]Rudd, C. D., Long, A. C., Kendall, K. N., and Mangin, C. G. E., *Liquid Moulding Technologies*, Elsevier, Cambridge, England, 1997.

[34]Beck, R., Driver, D., Wright, M., Laub, B., Hwang, H., Slimko, E., Edquist, K., Sepka, S., Wilcockson, W., and Thames, T., "Development of the Mars Science Laboratory Heatshield Thermal Protection System," *41st AIAA Thermophysics Conference*, Vol. 51, American Institute of Aeronautics and Astronautics, Reston, Virigina, jun 2014, pp. 1139–1150.

[35]Carman, P. C., *Flow of gases through porous media*, Academic Press, 1956.

[36]Tomadakis, M. M. and Robertson, T. J., "Viscous Permeability of Random Fiber Structures: Comparison of Electrical and Diffusional Estimates with Experimental and Analytical Results," *Journal of Composite Materials*, Vol. 39, No. 2, 2005, pp. 163–188.

[37]Maples, R. E., "Blending," *Petroleum Refinery Process Economics*, Penn Well Corporation, Oklahoma, 2nd ed., 2000.

[38]Šimáček, P. and Advani, S. G., "Desirable features in mold filling simulations for Liquid Composite Molding processes," *Polymer Composites*, Vol. 25, No. 4, aug 2004, pp. 355–367.